Int. J. Electrochem. Sci., 11 **(2016)** 967 - 982

International Journal of
ELECTROCHEMICAL
SCIENCE
www.electrochemsci.org

Noble Metal and Mn_3O_4 Supported Carbon Nanotubes: Enhanced Catalysts for Ethanol Electrooxidation

Suwaphid Themsirimongko[1], *Napapha Promsawan*[1], *Surin Saipanya*[1,2,*]

[1] Department of Chemistry, Faculty of Science, Chiang Mai University, Chiang Mai, 50200 Thailand
[2]Materials Science Research Centre, Faculty of Science, Chiang Mai University, 50200 Thailand
[*]E-mail: surin_saipanya@hotmail.co.uk

Received: 19 October 2015 / *Accepted:* 25 November 2015 / *Published:* 1 January 2016

The carbon nanotubes (CNT) were modified by Mn_3O_4 before deposition of metal catalysts (*e.g.* Pt and Pd) by improved polyol method. Crystallinity, morphology and composition of the synthesized electrocatalysts were characterized by Fourier transform infrared (FT-IR) spectroscopy, x-ray diffraction (XRD), transmission electron microscopy (TEM) and energy dispersive x-ray spectroscopy (EDS). It was found that the Mn_3O_4 nanoparticles are dispersed and covered the CNT surface. The various atomic ratios of 10 wt% Pt_xPd_y nanoparticles are also uniformly dispersed on Mn_3O_4-CNT with the particle size of 1 - 4 nm. Their electrocatalytic performances in ethanol oxidation were investigated by cyclic voltammetry (CV) and Chronoamperometry (CA). The prepared catalyst showed enhanced catalytic activity and more stability than the commercially available PtRu/Vulcan XC-72 catalyst. It is proposed that additions of metal oxides and noble metal could develop active sites for ethanol oxidation, which their catalytic performances were improved. These results imply that the prepared various atomic ratios Pt_xPd_y/Mn_3O_4-CNT nanocomposite could be a promising electrocatalyst to enhance performance of direct ethanol fuel cell applications.

Keywords: carbon nanotube(CNT); PtPd alloy; direct ethanol fuel cell; Manganese oxide

1. INTRODUCTION

Ethanol is used as fuel in direct ethanol fuel cells (DEFCs) reaction for numerous applications [1, 2, 3]. The ethanol is not toxic and easy to stock up and carry due to its high boiling point. It provides high energy density as using of 12 electrons transfer to complete an oxidation reaction. Moreover, it can be produced in huge quantities from raw farming products containing [3, 4, 5].

Nevertheless, the DEFCs technology has been obstructed by the slow ethanol oxidation reaction at the anode, owing to short of an active anode catalyst [2]. Moreover, small organic molecules are used as fuel can generate the poisoning species COads at anode site from surface

electro-oxidation reaction under the condition of acidic medium. Generally, Platinum (Pt) is used as catalyst in the electrochemical reaction of small organic fuel cell occurs *via* two pathway mechanisms [2, 5]. The majority desirable reaction path for direct ethanol fuel cells is *via* a dehydrogenation reaction, which does not produce carbon dioxide (CO) as oxidation reaction intermediate. The second reaction path is *via* dehydration, obtaining adsorbed CO as an intermediate. The carbon dioxide (CO_2) is generated by avoiding the adsorbed CO intermediate poisoning step, by this means enhancement of the overall turnover rate occurs.

Similar to the electro-oxidation mechanism of methanol, ethanol can be described by the following equations (equation 1-3) for the electrocatalytic oxidation of ethanol at Pt catalyst surface [1, 2, 5]:

Anode electrode: $C_2H_5OH + 3H_2O \rightarrow 2CO_2 + 12H^+ + 12e^-$ (1)

Cathode electrode: $3O_2 + 12H^+ + 12e^- \rightarrow 6H_2O$ (2)

Overall reaction: $C_2H_5OH + 3O_2 \rightarrow 2CO_2 + 3H_2O$ (3)

To reduce the poisoned catalyst as mentioned above and the production cost of the fuel cells, one of the key challenges is the development of catalysts with a lower content of Pt [2, 5, 6]. Binary and ternary Pt-based catalysts have been attracted our attention for choosing catalyst systems [7]. It has to be concerned some points for catalyst support selection for stabilizing the metal nanoparticles and prevention of their immediate agglomeration, a porous support can be used for metal nanoparticle preparation. These porous materials allow the high dispersion of metal nanoparticles onto their surface [8]. CNT as catalyst support for low-temperature fuel cells has attracted a lot of attention owing to their exclusive structures and properties such as high surface area, excellent electronic conductivity, strong mechanical properties and high stability [9, 10]. Although, the confront of gaining greatly dispersed metallic nanoparticles with controllable loadings on CNT still occurs. One approach to heal this problem is to transform the CNT surface before loading the metal nanoparticles. A variety of methods including oxidation in strong acids, sono-chemcial and electrochemical have been used [11, 12, 13]. Moreover, carbon based materials with conductive oxides such as ITO, TiO_2, WO_x, IrO_2 and SnO_2 has been studied for catalyst electrode improvement [7, 11].

In this work, Pt_xPd_y/Mn_3O_4-CNT nanocomposites were prepared by polyol method and characterized by FT-IR, XRD, TEM and EDX for determinations of functional group, crystallinity, morphology and compositions. Studies of their activity and stability for ethanol oxidation on the prepared catalysts were achieved by CV and CA.

2. EXPERIMENTAL

2.1 Materials

Multiwall carbon nanotubes (Bayer tubes C150P) are obtained from Bayer Material Science. $H_4Pt_2Cl_6.6H_2O$ and $PdCl_2$ are purchased from Merck. $Mn(CH_3COO)_2.4H_2O$ are obtained from Sigma-Aldrich and 10 wt% Nafion solution is brought from Fuel Cell Store. Deionized water was obtained from a Millipore Milli-Q water system.

2.1 Catalyst preparation

The Mn_3O_4 modified CNT were prepared by improvement of modified polyol process in one-step preparation. The mass content of Mn_3O_4 to CNT is 2:5 and used for all electrocatalyst preparation.

Various atomic ratios of bimetallic metal (10 wt% metal content; *e.g*. Pt and Pd) on manganese oxide (Mn_3O_4) functionalized carbon nanotubes (CNT) were prepared with ethylene glycol as reducing agent and stabilizer. For the synthesis of Pt decorated Mn_3O_4 carbon nanotubes catalyst, 40 wt% manganese oxides of manganese (II) acetate tetrahydrate and CNT were dispersed in EG 3:1 v/v ratio in ultrasonication for 30 min. The solution was refluxed at 120 °C for 1 hour. 10 wt% of $H_2PtCl_6.6H_2O$ solution was added, and the pH of the resultant mixture was then adjusted to 11 by drop wise addition of 1 M NaOH solution. The resulting product was cooled to room temperature and the suspension was centrifuged at 9000 rpm, for 15 min. The residue was washed with DI-water until neutral pH was obtained. Finally, the product was dried overnight at 65 °C in an oven. This electrocatalyst was designated as Pt/Mn_3O_4-CNT.

The Pd/Mn_3O_4-CNT, PtPd/Mn_3O_4-CNT, $PtPd_3$/Mn_3O_4-CNT and Pt_3Pd/Mn_3O_4-CNT electrocatalysts were prepared by using similar procedures as described above. The theoretical mass of Pt and Pd metal as mono- and bi-metallic in all composite electrocatalysts were fixed at 10 wt%. with ratio 1:1, 1:3 and 3:1.

2.2 Catalyst characterization

Fourier transforms infrared spectroscopy (FT-IR, TENSOR-27, Bruker) was used to interpret the chemical observation and principal functional groups of the prepared electrocatalysts. XRD (Rigaku Mini Fliex II) was used in order to identify structural characteristics and the alloy formation of the prepared electrocatalysts, using the Cu Kα ($\lambda = 0.15418$ nm) source. The sample identification was assisted by X'Pert HighScore Plus computer software. TEM and EDX (JEM-2010, JEOL) was employed to investigate the morphologies and chemical compositions of the electrocatalysts, respectively.

2.3 Electrochemical measurements

A glassy carbon electrode (GCE, 3.0 mm) was polished on the polishing cloth with alumina (Al_2O_3) size 1.0 and 0.3 μm, respectively. The catalyst ink was prepared as follows: 2 mg of the prepared electrocatalyst was dispersed in 1 mL mixed solution of (6.25 mL Nafion solution (5 wt%), 20 mL ethanol and 73.75 mL DI-water. After that, the catalyst was ultrasonically dispersed for 30 min. 5 μL of the catalyst ink was gradually dropped onto the glassy carbon electrode and dried completely under the lamp.

The electrochemical studies have been performed using a conventional three-electrode cell, including an Ag/AgCl (saturated KCl) electrode as the reference electrode, a Pt wire as the counter electrode. The working electrode was prepared by dropping the prepared catalysts ink on the polished glassy carbon electrode.

An eDAQ potentiostat (EChem software) was used for the electrochemical measurement. The electrochemical characterization of the catalyst electrodes was investigated in N_2 saturated 0.5 M H_2SO_4 solution at the potential region from -0.4 to 1.0 V at a scan rate of 50 mVs^{-1}. Also the activity of the catalyst electrodes for ethanol oxidation was measured in N_2 saturated 0.5 M CH_3CH_2OH + 0.5 M H_2SO_4 at the potential region from 0.0 to 1.0 V with a scan rate of 50 mVs^{-1}. Additionally, the electrochemical durability of electrocatalysts was measured by using chronoamperometer (CA) at a fixed potential of 0.25 V for 3600 second.

3. RESULTS AND DISCUSSION

Mn_3O_4 nanoparticles loaded on the CNT (Mn_3O_4-CNT) and metal nanoparticles decorated on the Mn_3O_4-CNT (Pt/Mn_3O_4-CNT, Pd/Mn_3O_4-CNT and Pt_xPd_y/Mn_3O_4-CNT) were well prepared and characterized as follows:

3.1 Fourier transforms infrared spectroscopy (FT-IR)

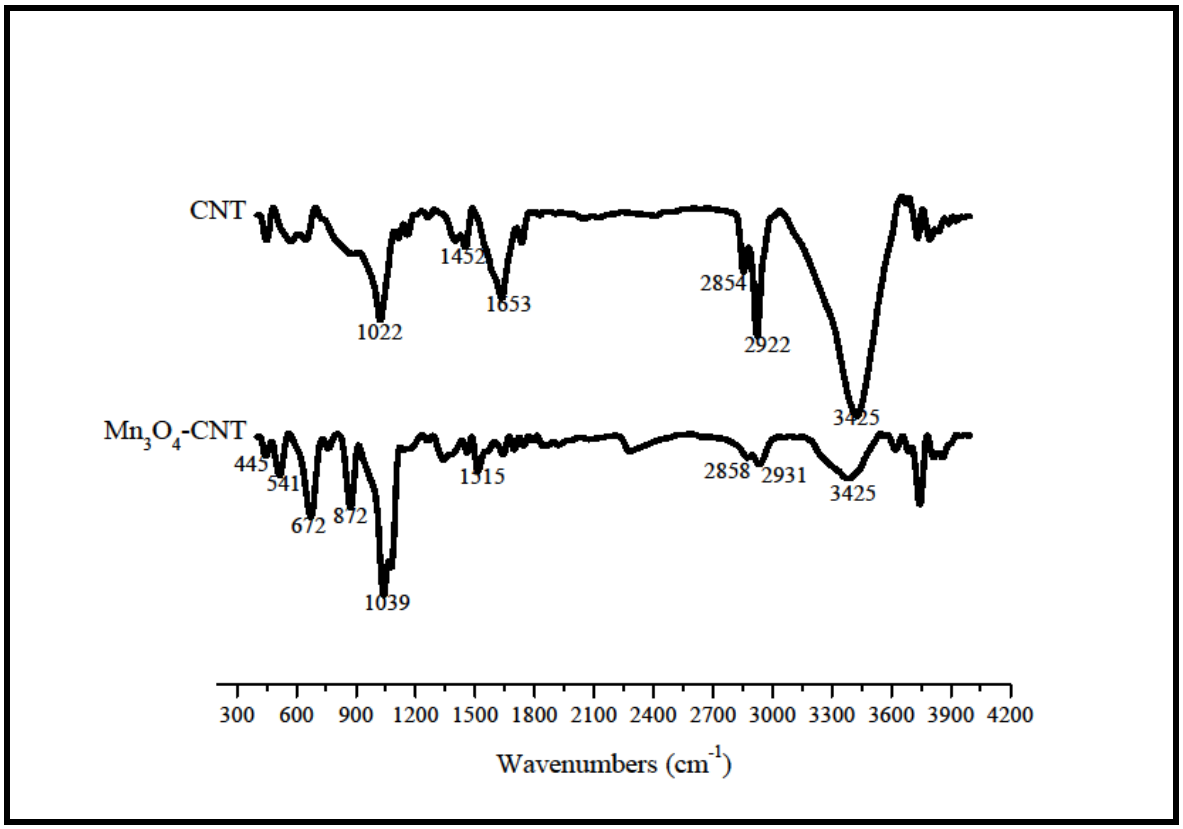

Figure 1. FT-IR spectra of CNT and Mn_3O_4-CNT nanocomposites.

The FT-IR spectra of CNT and synthesized Mn_3O_4-CNT nanocomposite materials in the range of 4000-400 cm^{-1} are shown in Figure 1. The broad bands observed at 3425 cm^{-1} are assigned to the intermolecular hydrogen bonding of hydroxyl groups (-OH) in CNT and Mn_3O_4-CNT. The Mn-O

stretching vibration band appears at 672 cm^{-1} corresponding to a tetrahedral site. Similarly, the vibration band at 541 cm^{-1} is directly related to distortion vibration of Mn-O in an octahedral site, and the absorption signal at 445 cm^{-1} corresponds to the bending vibration mode of both sites [14, 15]. The absorption bands at 1653, 1515 and 1452 cm^{-1} are spectral characteristic of C=C vibration of aromatics and C-O vibration of carboxyl group. In addition, the absorption bands at 1039 or 1022 cm^{-1} are not only attributed to the subsistence of C-O of alkoxy groups but also assigned to Mn-O-H vibrations. Furthermore, the vibration bands at 872, 2931 and 2858 cm^{-1} could be ascribed to the methylene (-CH_2) and methine (-CH) groups [16, 17, 18].

3.2 X-ray diffraction (XRD)

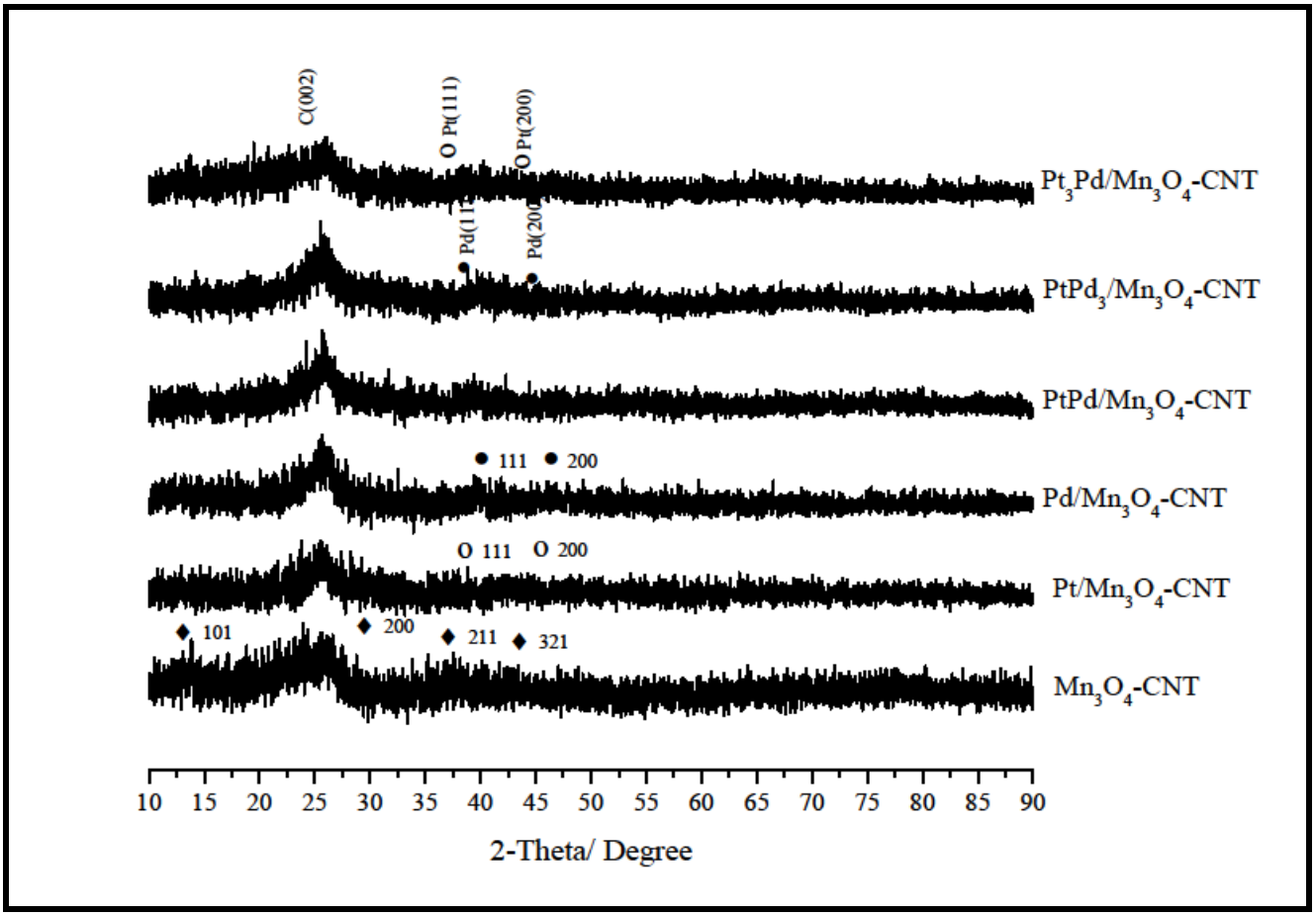

Figure 2. XRD patterns of Mn_3O_4-CNT, Pt_x/Mn_3O_4-CNT and Pd/Mn_3O_4-CNT and Pt_xPd_y/Mn_3O_4-CNT catalysts.

The phase purity and crystalline structure of the catalytic nanoparticles were characterized by XRD techniques in the 2θ range of 10 – 90° in Figure 2. The presence of broadening diffraction peaks at around 26° in all catalysts is assigned to the hexagonal graphite crystallographic planes (002) in CNT [19]. Although, all the XRD diffraction peaks of catalyst nanoparticles are undistinguished but it can be confirmed by X' Pert HighScore Plus software compared with the standard values of single

phase of CNT, Pt, Pd and Mn_3O_4 (Hausmannite) as JCPDS No. 00-008-0415, No. 00-004-0802, No. 00-005-0681 and No. 00-001-1127, respectively. From the XRD pattern of Mn_3O_4-CNT, diffraction peaks at 18, 31, 36, 44, 51, 54 and 64 correspond to crystalline planes of Mn_3O_4 (101), (200), (211), (220), (105) and (314), respectively. The XRD pattern of Pt/Mn_3O_4-CNT catalyst shows diffraction peaks at 39.8, 46.2 and 67.5 which can be attributed to the (111) (200) and (220) crystalline planes of the face-centered cubic (fcc) structure. For Pd/Mn_3O_4-CNT catalyst, the main diffraction peaks at 40.1and 46.7 are assigned to (111) and (200) crystalline planes of the face-centered cubic (fcc) structure, respectively [17, 18]. The less intensity of diffracted peaks may imply the low crystallinity of the prepared catalysts. This is attributed to smaller crystallie size of mono and bi-metallic catalysts supported on Mn_3O_4-CNT [20]. Metallic particles as expected from Scherrer equation after background subtraction, the average metallic particle sizes were calculated as shown in Table1. However, morphology and dispersion situation can also be confirmed in TEM characterization [16, 21].

Table 1. Summary of experimental XRD and TEM results for Pt_xPd_y/Mn_3O_4-CNT catalysts.

Catalysts	Peak	d-XRD (nm)	TEM (nm)
Pt/Mn_3O_4-CNT	220	1.56	1.2 ± 0.4
Pd/Mn_3O_4-CNT	111	2.75	3.1 ± 0.9
PtPd/Mn_3O_4-CNT	200	1.70	3.2 ± 0.8
$PtPd_3$/Mn_3O_4-CNT	111	1.60	2.1 ± 0.8
Pt_3Pd/Mn_3O_4-CNT	111	2.51	2.6 ± 0.7
Mn_3O_4-CNT	103	3.28	4.3 ± 1.1

3.3 Transmission electron microscopy (TEM)

The CNT was modified with Mn_3O_4 nanoparticles using ethylene glycol (EG) acting as reducing agent and stabilizer (in alkaline media) to control particles growth and prohibit agglomeration. Figure 3(a) shows the typical TEM of Mn_3O_4-CNT. It can be seen that Mn_3O_4 nanoparticles reveal rather dispersed on the surface of functionalized carbon nanotubes with a size distribution of 4.3 ± 1.1 nm, which are rather similar to the crystallite size calculated from XRD pattern, however some are agglomerated. It should be marked that the interaction between CNT and metal nanoparticles was strong as the metal nanoparticles could not be removed by wash and harsh stirring [15, 22].

Figure (b)-(f) shows the TEM of mono and bimetallic catalysts supported on Mn_3O_4-CNT, respectively. Approximate 100 metal nanoparticles were examined and the results are given in Table 1

and these results confirm and fairly agree with the value of the crystallite size calculated from XRD data.

Those TEM images show the successful attachment of mono-, bi-metallic nanoparticles to the Mn_3O_4-CNT. Moreover, the EDS results (not showed here for brevity) reveals the presence of chemical compositions of the metal catalysts.

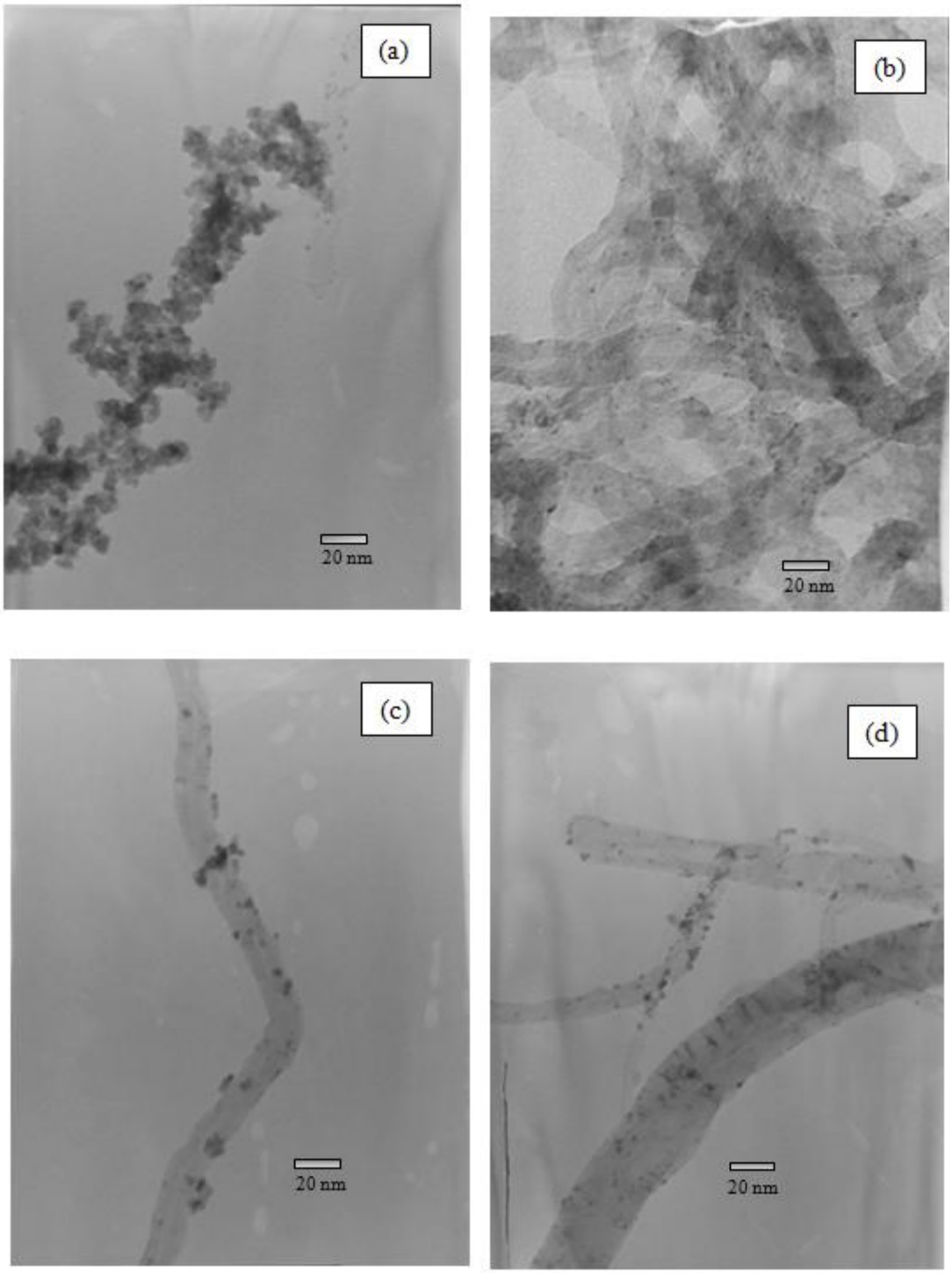

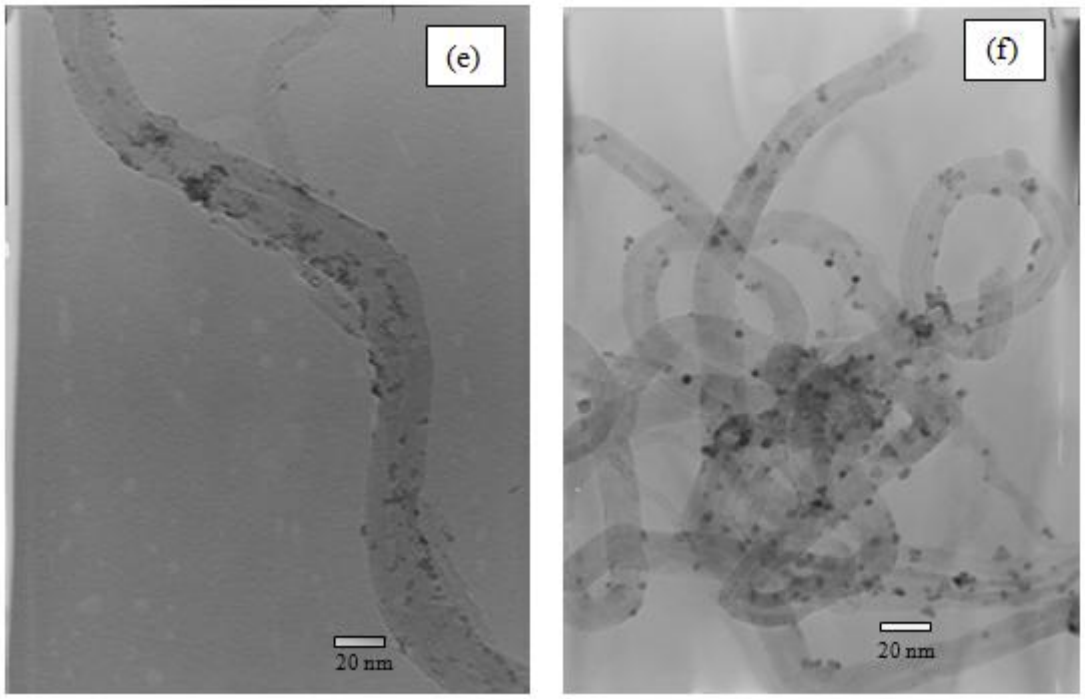

Figure 3. TEM images of (a) Mn_3O_4-CNT, (b) Pt_x/Mn_3O_4-CNT, (c) Pd/Mn_3O_4-CNT, (d) $PtPd_3/Mn_3O_4$-CNT, (e) $PtPd/Mn_3O_4$-CNT and (f) Pt_3Pd/Mn_3O_4-CNT.

3.4 Electrochemical characterization

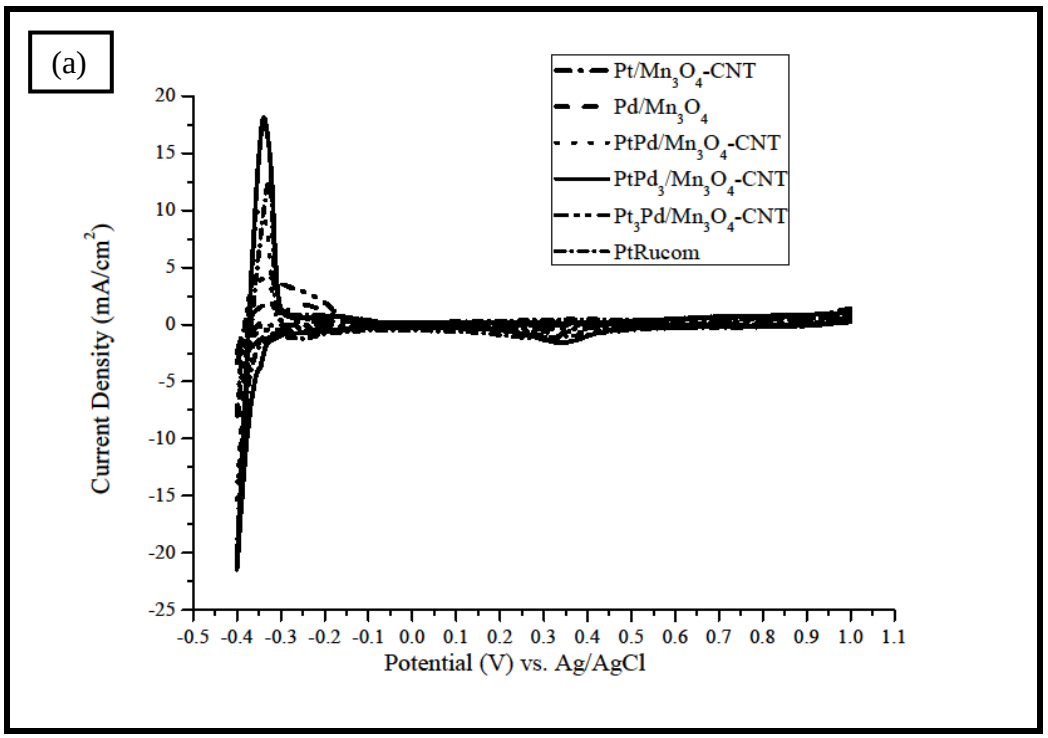

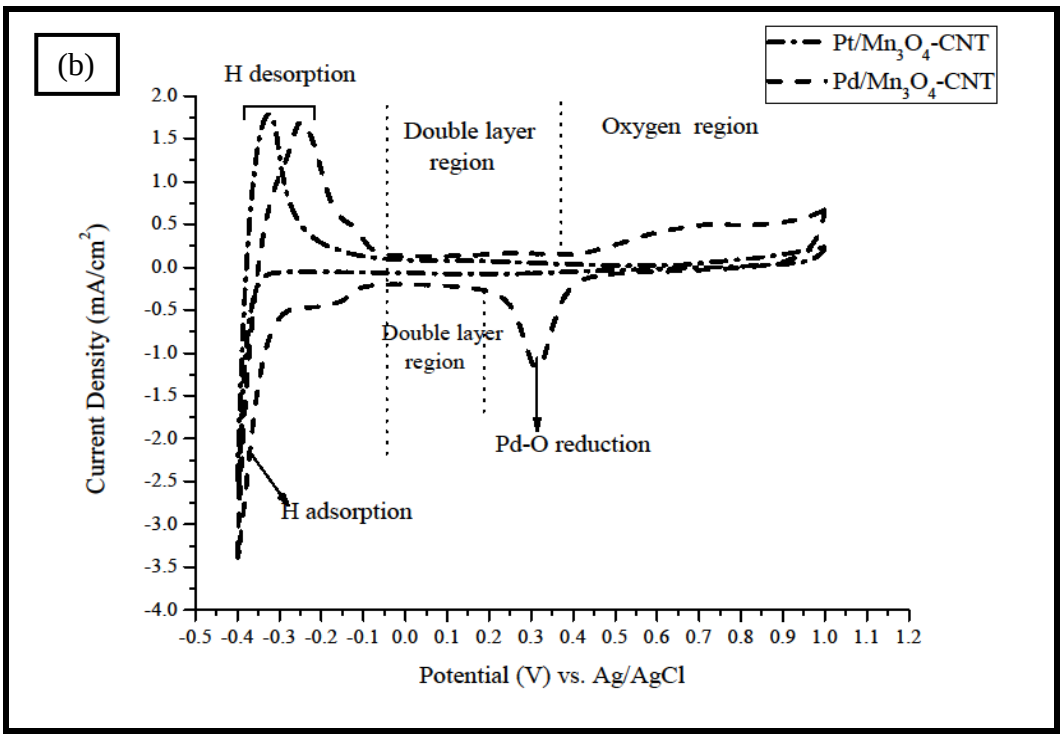

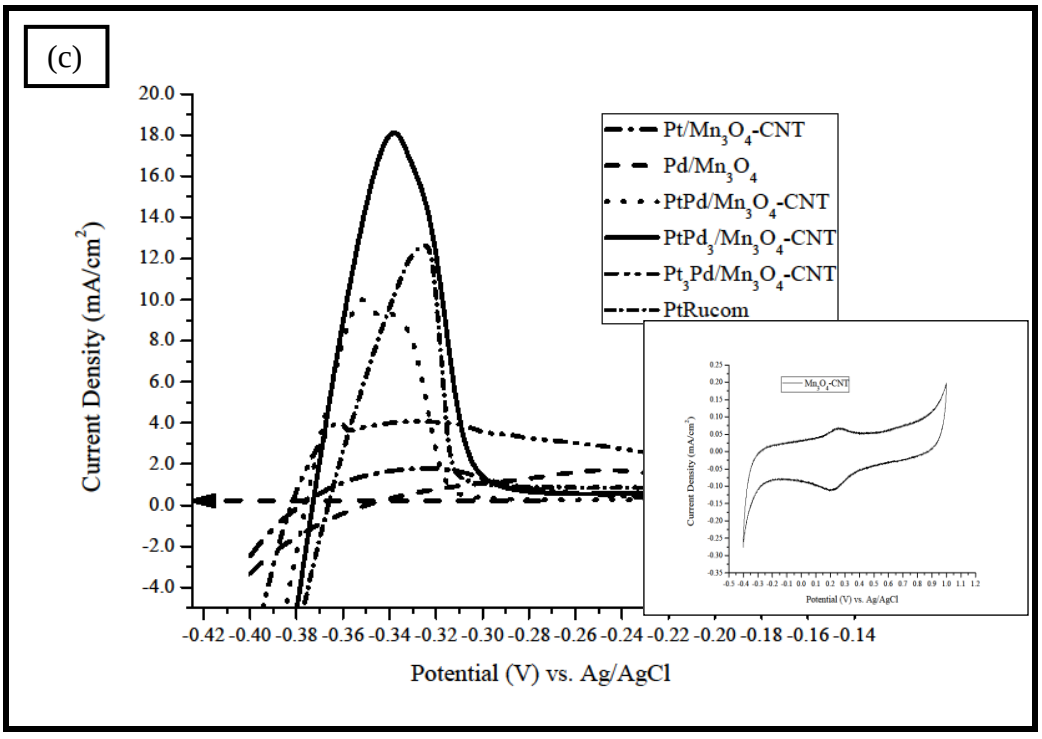

Figure 4. Cyclic voltammograms of (a) all catalysts and (b) Pt_x/Mn_3O_4-CNT and Pd/Mn_3O_4-CNT and (c) specific area of CVs of all catalysts.

The CV of 10 wt% various atomic ratios $Pt_xPd_yMn_3O_4$–CNT and commercial PtRu/C electrocatalysts in a nitrogen saturated 0.5 M H_2SO_4 aqueous solution at scan rate of 50 mVs^{-1} were studied (Figure 4 (a)-(c)). The CVs visibly disclose the characteristic peaks of hydrogen

adsorption/desorption, double layer, metal oxide (of Pt, Pd) formation and metal oxides reduction on their catalyst surfaces. The peaks in the -0.4 to -0.2 V potential region of forward scan as well as reverse scan are signs of underpotential deposition of hydrogen (H_{upd}) as a result of adsorption/desorption processes. Moreover, the peaks beyond 0.30 V during the anodic scan and 0.55 to 0.15 V in the reverse scan are characteristics of individual formation and reduction on the surfaces of the electrode indicating to the redox reactions with products of some $Pt(OH)x.nH_2O$, $Pd(OH)_x.nH_2O$ and $Mn(OH)_2$ (where x = 2, 4) [9, 23, 24].

On the other hand, at the voltammetric manner in the H_{upd} regions confirms possible differences in the hydrogen adsorption/desorption processes, which can be associated with the distinctions in the structural and crystallographic characteristics of dissimilar surfaces of the Pt, Pd and Pt_xPd_y catalysts supported on the Mn_3O_4 functionalized carbon nanotubes. It was stated the broad peaks might consist of (110) and (100) of hydrogen surfaces, and anions on (111) Pt surface on catalysts which designates some Pt crystallites with no specifically exposed crystal in spherical shape [24, 25]. Furthermore, the H adsorption/desorption peaks with high current densities in the H_{upd} peaks of Mn_3O_4 promoted Pt_xPd_y/CNT, Pt/CNT and Pd/CNT as compared with commercial PtRu/C sample clearly suggests a higher amount of specifically exposed clean Pt surfaces. Therefore, proportion of Pt and Pd in bimetallic catalysts has affected to electrochemically active surface area and cooperation of Pd and Mn_3O_4 that could possible to promote the electrocatytic activity in electro-oxidation reaction.

3.4.1 Ethanol Electrooxidation

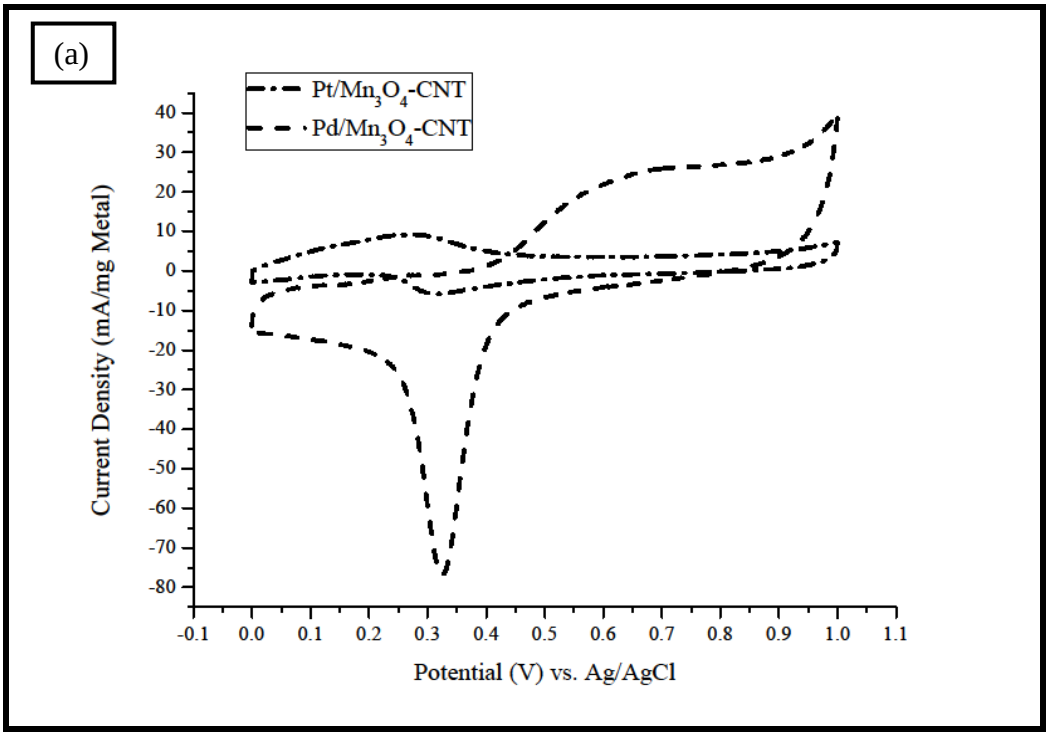

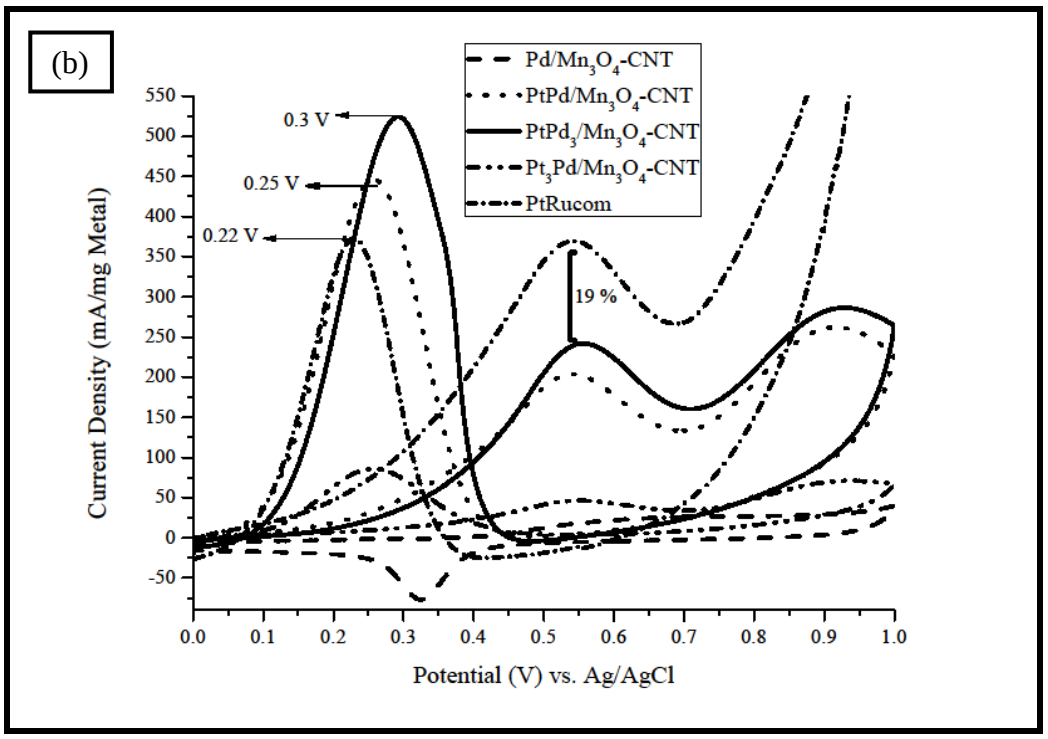

Figure 5. Cyclic voltammograms of (a) Pt_x/Mn_3O_4-CNT and Pd/Mn_3O_4-CNT and (b) Pt_xPd_y/Mn_3O_4-CNT catalysts recorded in 0.50 M H_2SO_4 aqueous solution containing 0.50 M CH_3CH_2OH at a scan rate of 50 mVs^{-1}.

Ethanol electrooxidation is a complex reaction and it can lead to poisoning of pure Pt suface due to adsorption of intermediates and poisonous species during oxidation. An entire ethanol oxidation discharges 12 electrons per molecule and the C-C bond is broken. Experimental studies have revealed that ethanol is partially oxidized to acetaldehyde and acetic acid (2 – 4 electron in oxidation reactions) instead of fully oxidized (12 electron in oxidation reactions) [12]. Consequently, the ethanol electrooxidation was considered to require more active and selective catalysts to complete the reaction.

Ethanol oxidation on our prepared catalysts was monitored by CV measurement in a nitrogen-saturated 0.5 M CH_3CH_2OH + 0.5 M H_2SO_4 solution, and the results are compared with the commercial PtRu/C, shown in Figure 5. It is clear that the addition of either Pd or Mn_3O_4 lead to a promoting effect in ethanol oxidation. The CVs of mono metallic catalysts, Pt/Mn_3O_4-CNT and Pd/Mn_3O_4-CNT, show diminutive oxidation and reduction peaks shown in Figure 5 as the enhancement of Mn_3O_4 nanoparticles promoted Pt and Pd on functionalized carbon nanotubes catalysts, while the amount of oxygenated peak of Mn_3O_4-OH is observed at 0.33 V [12].

The Pd/Mn_3O_4-CNT clearly showed the reduction of the Pd-OHads and $Mn(OH)_2$ species and presence of reduction peaks (0.33 V) and peaks current density indicating the formation of oxygenated on Pd and Mn_3O_4 species which are from the water and ethanol activations. However, more oxides or oxygenated species (oxophilicity; $M(OH)_x$ or MO_x) result in retardation of the electrocatalytic activity for oxidation reaction of Pt base catalysts [23].

The efficiencies of the Pt and different Pt_xPd_y bimetallic catalysts supported on high specific surfaces area Mn_3O_4-CNT and commercial PtRu/C catalysts on ethanol oxidation were compared

concerning oxidation potential, onset potential, forward and backward oxidation peak current density, the ratio of the forward peak (If) to the backward peak (Ib); these data are shown in Table 2.

Table 2. Comparison of various metal/Mn_3O_4-CNT electrocatalysts on ethanol oxidation.

Catalysts	Mole ratios	Forward anodic sweep		Reverse anodic sweep		Onset potential	I_b/I_f Ratio	Stability at 3600 s
		I_f(mA/mg Metal)	E_{max} (V)	I_b(mA/mg Metal)	E_{max} (V)	E (V)		mA/mg Metal
Pt/Mn_3O_4-CNT	1	-	-	-	-	-	-	-
Pd/Mn_3O_4-CNT	1	-	-	-	-	-	-	-
PtPd/Mn_3O_4-CNT	1:1	200	0.540	450	0.259	0.125	2.25	0 at 2200 s
$PtPd_3$/Mn_3O_4-CNT	1:3	235	0.529	540	0.301	0.125	2.30	3.7
Pt_3Pd/Mn_3O_4-CNT	3:1	45	0.521	84	0.285	0.125	1.88	4.4
PtRu/Vulcan	1:1	349	0.550	346	0.249	0.075	0.99	-4.3

Typical voltammetry of two oxidation peaks show in all CV curves. The peak in the forward peak was related to the ethanol oxidation, and another one in the reverse peak was mainly associated with the elimination of the remaining carbonaceous species from the forward scan [25]. On the other hand, the current density during the anodic scan raise gradually at lower potentials and then increases quickly until a current peak is obtained. After backward scan, a reactivation is obtained on the electrode. The peaks at approximate 0.55 V are ascribed to ethanol oxidation, forming CO_2 and adsorbed carbonaceous species (principally as CO). This adsorbed CO causes the loss of catalyst activity. The oxidation peaks of backward scan at ca. 0.30 V can attribute to oxidations of the adsorbed carbonaceous species and ethanol to CO_2. Although, the forward anodic peak current density of commercial PtRu catalysts is higher than that of synthesized $PtPd_3$/Mn_3O_4-CNT catalysts about 19 % but reversed anodic peak is less than the prepared catalyst that implies the prepared catalysts can proficiently eliminate intermediates more than commercial PtRu/C.

However, the onset potential, the commercial PtRu catalysts is rather similar to the prepared catalysts (ca. 0.08 V). The ratio of Ib to If is regularly utilized to estimate the catalyst tolerance. Basically, a higher Ib/If value represents a relatively complete oxidation of ethanol, producing CO_2. The ratios for $PtPd_3$/Mn_3O_4-CNT, PtPd/Mn_3O_4-CNT, Pt_3Pd/Mn_3O_4-CNT and PtRu/C nanocomposites are 2.30, 2.25, 1.88 and 0.99, respectively, implying that Pt_xPd_y bimetallic catalysts supported on Mn_3O_4 functionalized CNT have much supplementary tolerance toward carbonaceous species poisoning and cause more complicated oxidation of ethanol [12].

3.4.2 Electrocatalyst stability

Chronoamperometric (CA) measurements were carried out in an electrolyte of 0.5 M CH_3CH_2OH + 0.5 M H_2SO_4 with a bias potential of 0.25 V for duration 3600 s as shown in Figure 6. The current-time curves of all catalysts display quickly decay at the initial stages which are attributed

to the accumulation of poisonous intermediates, such as COads, generated from the continuous oxidation of ethanol on the catalyst surface [14,20, 26] .

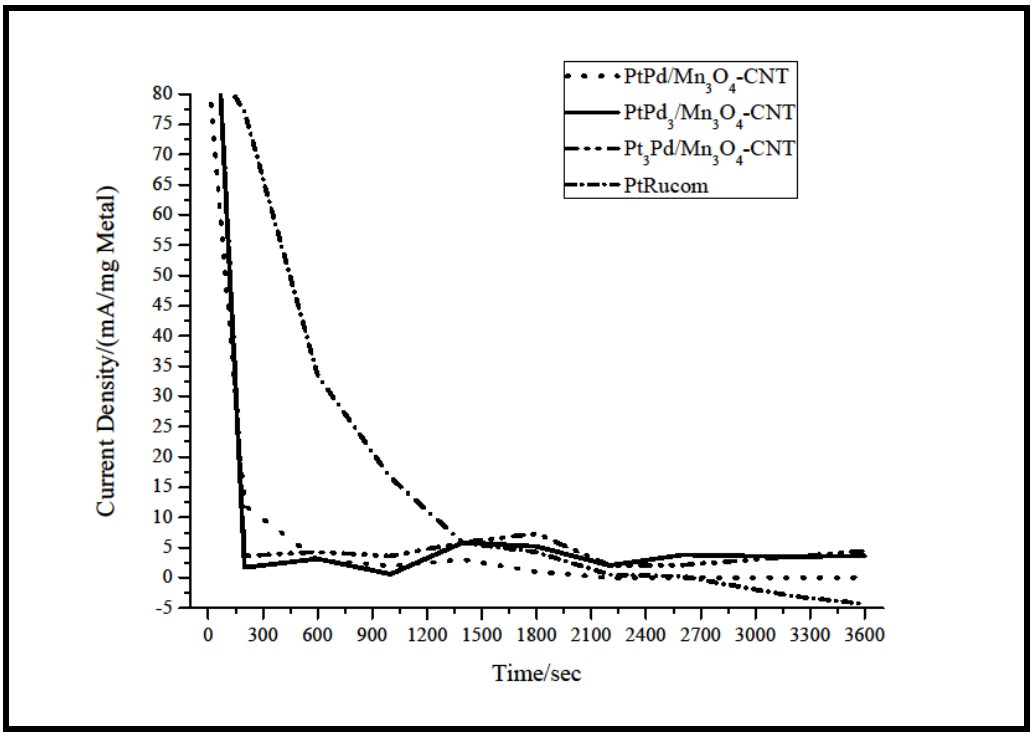

Figure 6. Chronoamperograms of various Pt_xPd_y/Mn_3O_4-CNT catalysts recorded in 0.50 M H_2SO_4 aqueous solution containing 0.50 M CH_3CH_2OH obtained for 3600 s at 0.25 V.

After the catalytic reactions reach a steady state in which the adsorptions oxygenated species and CO-like species occur [27]. Moreover, increases in initial and limiting current densities is obviously found after the addition of Pd and Mn_3O_4 in the catalysts. The current densities for the prepared catalysts are higher than that for commercial PtRu/C composites during the whole experimental range. The current density of Pt_3Pd/Mn_3O_4–CNT catalyst in ethanol oxidation is the highest when compared with the other three catalysts and also the commercial PtRu/C catalyst. This can be indicated that COads tolerance or other poisonous intermediates can be removed when Pd and Mn_3O_4 were added.

The presences of Pd and Mn_3O_4 in catalysts can prove the enhancement the proton conductivity of the catalysts, which can promote the electrocatalytic oxidation of ethanol *via* dehydrogenation in ethanol oxidation [20].

It has been reported that the electrocatalytic activity increases with the increase of the exchange rate of H^+ ions [9], which can be promoted by the presence of Mn_3O_4 because MnOOH, Mn_2O_3 and MnO_2 can be generated by reactions of proton and Mn_3O_4(equation 4-7). The active Mn^{3+}/Mn^{2+} redox couples can effectively catalyze the dehydrogenation of ethanol and further promote the electrocatalytic activity, which are similar to the “hydrogen spillover effect” in Pt-SnO_2 system [25]. The possible mechanisms stated as follows:

$$M\ (Pt, Pd)\text{-}Mn_3O_4 + CH_3CH_2OHads \rightarrow \ldots \rightarrow M\text{-}COads + MnOOH \quad (4)$$

$$MnOOH \rightarrow MnO_2 + H^+ + e^- \quad (5)$$

$$M\text{-}MnO_2 + H_2O \rightarrow M\text{-}OHads + MnOOH \quad (6)$$

$$M\text{-}OHads + M\text{-}COads \rightarrow 2M + CO_2 + H^+ + e^- \quad (7)$$

where "…." stand for the processes of the C-C bond splitting

Apparently, OHads species is necessary for removal of adsorbed CO on Pt [20, 22, 24]. Those strongly adsorbed intermediates (-CO species) such as CH_3-CO and CH-CO, are also easily adsorbed on the catalyst surface in the electrooxidation. The other possible intermediate reactions can be occurred as there are some species of Pt, Pd on the surfaces of the catalysts (equation 8-19).

$$CH_3\text{-}CH_2OH + Pt \rightarrow Pt\text{---}(CHOH\text{-}CH_3)ads + H^+ + e^- \quad (8)$$

$$Pt\text{---}(CHOH\text{-}CH_3)ads \rightarrow Pt + CHO\text{-}CH_3 + H^+ + e\text{-} \quad (9)$$

$$Pt + CHO\text{-}CH_3 \rightarrow Pt\text{---}(CO\text{-}CH_3)ads + H+ + e\text{-} \quad (10)$$

$$Pt\text{---}(CO\text{-}CH_3)ads + Pt\text{---}(OH)ads \rightarrow 2Pt + CH_3\text{-}COOH \quad (11)$$

$$Pt\text{---}(CO\text{-}CH_3)ads + Pt \rightarrow Pt\text{---}(CO)ads + Pt\text{---}(CH_3)ads \quad (12)$$

$$Pt\text{---}(CH_3)ads + Pt\text{---}(H)ads \rightarrow 2Pt + CH_4 \quad (13)$$

$$Pt - COads + H_2O \rightarrow CO_2 + 2H^+ + Pt \quad (14)$$

$$Pt + H_2O \rightarrow Pt\text{---}OHads + H^+ + e^- \quad (15)$$

$$Pd + H_2O \rightarrow Pd\text{---}OHads + H^+ + e^- \quad (16)$$

$$Mn_3O_4 + H_2O \rightarrow Mn_3O_4\text{---}OHads + H^+ + e^- \quad (17)$$

$$CH_3CH_2\text{-}OH + Mn_3O_4 \rightarrow Mn_3O_4\text{---}OHads + H_3C\text{-}C^+H_2 \quad (18)$$

$$Pt\text{---}COads + (Pt, Pd \text{ or } Mn_3O_4)\text{---}OHads \rightarrow Pt + X + CO_2 + H^+ + e^- \quad (19)$$

Both of Pd and manganese oxides provides OH- ion to oxidize the adsorbed intermediates on Pt surface [17, 28]. Moreover, the inherent Mn-OH bonds in the hydrous Mn_3O_4 can also donate the hydroxide species to oxidize the adsorbed poisoning species. So, the Mn_3O_4 and Pd can effectively promote the dehydrogenation of ethanol oxidation and remove the adsorbed intermediates to release the Pt active sites. Thus, the Pt_xPd_y/Mn_3O_4-CNT exhibits enhanced electrocatalytic activity, excellent stability and anti-poisoning ability toward ethanol oxidation.

Pt-base bimetallic materials are the most commonly used as electrocatalysts in the electrochemical oxidation of small molecules because of their excellent properties in the adsorption and dissociation [28]. Nevertheless, the enhanced current in Pt-based alloys is from acetaldehyde and/or acetic acid formations than from the C-C bond cleavage. Whereas Pt is the active metal for C-C activation, these alloyed catalysts with reduced surface Pt truly lower the overall conversion to CO_2. In a noble metal binary system, higher transition metal content can generate more complexes of transition metal and OH_{ads} species, resulting in water dissociation, which assist the oxidation of small molecules, adsorbed the catalyst surfaces. Though, higher transition metal content could also diminish the occupancy of active noble metal atoms on the surface, and consequently impair the whole performance of dissociation of the adsorbed molecules.

4. CONCLUSION

Preparation of Pt_xPd_y bimetallic catalysts supported Mn_3O_4 functionalized carbon nanotubes *via* modified polyol method was performed and the prepared catalysts were obtained uniformly dispersed. An improvement of electroactivity capability was studied by optimizing the ratio of Pt and Pd on Mn_3O_4-CNT for the ethanol oxidation. It was found that the presence of noble metal and Mn_3O_4 in catalysts could enhance the electrocatalytic activity toward ethanol oxidation from CV and CA results. Thereofore, it could be pointed out that the interaction between the Pt and Pd metal nanoparticles and oxygenated groups from metal oxide on the supports significantly improved the ethanol electrooxidation performance with high current densities and extended stability.

ACKNOWLEDGEMENTS
The authors are grateful to thank CMU- Mid- Career Research Fellowship program for financial support and Energy Research and the Technology and the National Research University Project under Thailand's Office of the Higher Education Commission and Development Institute-Nakornping Chaing Mai University for experimental support.

References

1. C. Lamy, E. M. Belgsir and J. M. Léger, *J. Appl. Electrochem.*, 31 (2001) 799.
2. C. Lamy and C. Coutanceau, Chapter 1 Electrocatalysis of Alcohol Oxidation Reactions at Platinum Group Metals, in: Catalysts for Alcohol-Fuelled Direct Oxidation Fuel Cells, The Royal Society of Chemistry, United Kingdom, 2012.
3. A. O. Neto, R. R. Dias, M. M. Tusi, M. Linardi and E.V. Spinacé, *J. Power Sources*, 166 (2007) 87.
4. E. Antolini, *J. Power Sources*, 170 (2007) 1.
5. J. Friedl and U. Stimming, *Electrochim. Acta*, 101 (2013) 41.
6. A. R. Bonesi, M. S. Moreno, W. E. Triaca and A. M. C. Luna, *Int. J. Hydrogen Energy*, 35 (2010) 5999.
7. Y. -C. Chiang, W. -H. Lin and Y. -C. Chang, *Appl. Surf. Sci*., 257 (2011) 2401.
8. C. -W. Liu, Y. -W. Chang, Y. -C. Wei and K. -W. Wang, *Electrochim. Acta*, 56 (2011) 2574.
9. S. K. Meher and G. R. Rao, *J. Phys. Chem. C*, 117 (2013) 4888.
10. M. S. Saha and A. Kundu, *J. Power Sources*, 195 (2010) 6255.
11. S. Sha rma and B. G. Pollet, *J. Power Sources*, 208 (2012) 96.
12. E. V. Spinacé, A. O. Neto, T. R. R. Vasconcelos and M. Linardi, *J. Power Sources*, 137 (2004) 17.
13. S. Yin, Q. Zhu, Y. Qiang and L. Luo, *Chin. J. Catal*., 33 (2012) 290.
14. Z. Ji, X. Shen, G. Zhu, K. Chen, G. Fu and L. Tong, *J. Electroanal. Chem.*, 682 (2012) 95.
15. L. Laffont and P. Gibot, *Mater. Charact.*, 61 (2010) 1268.
16. K.A.M. Ahmed, Q. Zeng, K. Wu and K. Huang, *J. Solid State Chem.*, 183 (2010) 744.
17. Y. Zhao, S. Nie, H. Wang, J. Tian, Z. Ning and X. Li, *J. Power Sources*, 218 (2012) 320.
18. Z.-H. Wang, L.-X. Yuan, Q.-G. Shao, F. Huang and Y.-H. Huang, *Mater. Lett.*, 80 (2012) 110.
19. X. Yang, X. Wang, G. Zhang, J. Zheng, T. Wang, X. Liu, C. Shu, L. Jiang and C. Wang, *Int. J. Hydrogen Energy*, 37 (2012) 11167.
20. J. Cai, Y. Huang, B. Huang, S. Zheng and Y. Guo, *Int. J. Hydrogen Energy*, 39 (2014) 798.
21. Y. Zhao, W. Ran, D. -B. Xiong, L. Zhang, J. Xu and F. Gao, *Mater. Lett.*, 118 (2014) 80.
22. G. S. Gund, D. P. Dubal, B. H. Patil, S. S. Shinde and C. D. Lokhande, *Electrochim. Acta*, 92 (2013) 205.

23. J. Yin, S. Shan, M. S. Ng, L. Yang, D. Mott, W. Fang, N. Kang, J. Luo and C. -J. Zhong, *Langmuir*, 29 (2013) 9249.
24. K. V. Sankar, S. T. Senthilkumar, L. J. Berchmans, C. Sanjeeviraja and R. K. Selvan, *Appl. Surf. Sci.*, 259 (2012) 624.
25. Y. Li, W. Gao, L. Ci, C. Wang and P. M. Ajayan, *Carbon*, 48 (2010) 1124.
26. J. Ma, H. Sun, F. Su, Y. Chen, Y. Tang, T. Lu and J. Zheng, *Int. J. Hydrogen Energy*, 36 (2011) 7265.
27. Y. Huang, J. Cai and Y. Guo, *Int. J. Hydrogen Energy*, 37 (2012) 1263.
28. A. Brouzgou, A. Podias and P. Tsiakaras, *J. Appl. Electrochem.*, 43 (2013) 119.